Published in final edited form as:
AIAA J. 2019 April ; 57(4): 1725–1735. doi:10.2514/1.J057229.

Volterra Kernels Assessment via Time-Delay Neural Networks for Nonlinear Unsteady Aerodynamic Loading Identification

Natália C. G. de Paula[*],
São Carlos School of Engineering, University of São Paulo, São Carlos, SP, 13566-590, Brazil

Flávio D. Marques[†],
São Carlos School of Engineering, University of São Paulo, São Carlos, SP, 13566-590, Brazil

Walter A. Silva[‡]
NASA Langley Research Center, Hampton, VA, 23681-0001, United States

Abstract

Reduced-order modeling using the Volterra series approach has been successfully applied in the past decades to weakly nonlinear aerodynamic and aeroelastic systems. However, aspects regarding the identification of the kernels associated with the convolution integrals of Volterra series can profoundly affect the quality of the resulting reduced-order model (ROM). An alternative method for their identification based on artificial neural networks is evaluated in this work. This relation between the Volterra kernels and the internal parameters of a time-delay neural network is explored for the application in the reduced-order modeling of nonlinear unsteady aerodynamic loads. An impulse-type Volterra-based ROM is also under consideration for comparison. All aerodynamic data used for the construction of the reduced-order models are obtained from computational fluid dynamics (CFD) simulations of the NACA 0012 airfoil using the Euler equations. Prescribed inputs in pitch and in plunge degrees of freedom at different free-stream Mach numbers are used to evaluate the range of applicability of the obtained models. For weakly nonlinear test cases, the modeling performance of the neural network Volterra ROM was comparable to the impulse-type ROM. Additional accuracy and adequate modeling of stronger nonlinearities, however, could only be attained with the inclusion of the neural network kernels of higher-order in the Volterra ROM. A generic expression is derived for the kernel function of p^{th}-order from the internal parameters of a time-delay neural network.

II. Introduction

REDUCED-ORDER model (ROM) is a concept that has been extensively explored in nonlinear unsteady aerodynamics with the widespread use of computational fluid dynamics (CFD) codes. Although CFD is a powerful tool for modeling complex flow features, especially those appearing in the transonic flight regime, the resulting models with thousands or millions of degrees of freedom are computationally demanding. Such costs are

[*]Graduate Student, Department of Mechanical Engineering, natalia.cg.paula@gmail.com.
[†]Associate Professor, Department of Mechanical Engineering, AIAA Member.
[‡]Senior Research Scientist, Aeroelasticity Branch, AIAA Associate Fellow.

unfeasible at early design phases or for multidisciplinary design problems [1]. ROMs are relatively more simple mathematical models that represent a viable alternative to more readily interpret a complex system behavior and to perform additional quantitative analyses more quickly. Extensive reviews of order reduction techniques focused on their application in aeroelasticity are given in Refs. [1] and [2].

This work concentrates on a specific class of reduced-order models based on system identification techniques, to which Volterra series and artificial neural networks belong. Both methods map the relation between the output and the input of a nonlinear system. In fact, for some specific neural network architectures, they can be related through the association of the kernels in a Volterra series with the internal parameters of a trained neural network. Such a relation has been well established for nonlinear dynamic systems in general [3–5], but not extensively explored for the modeling of unsteady aerodynamic loads.

Volterra series [6] offer a convenient mathematical representation of nonlinear systems through multidimensional convolution integrals, each associated with a kernel function. These higher-order kernels can be seen as extensions of the linear impulse response to multiple dimensions. Classical identification of Volterra kernels involves exciting the system with a series of steps or impulses of various orders. Its application to weakly nonlinear aerodynamic and aeroelastic systems is well established [7–9]. This technique, however, lacks robustness in respect to the choice of the excitation parameters [8] and is limited to the identification of low-order kernels, i.e., usually up to second-order. Other identification methods based on more general input-output relations include a least-squares approach through pseudo-inverses [10, 11] and kernel approximations using multiwavelet constructions [12, 13].

The synthesis of Volterra kernels can be a computational resource-intensive procedure, especially when it comes to higher-order kernels and representation of stronger nonlinearities. Moreover, proper identification of the cross-couple existing when multiple degrees of freedom of a nonlinear system are simultaneously excited represents another problem concerning the application of Volterra-based ROMs to transonic aerodynamics [2]. These limitations have been addressed in some recent efforts directed toward the use of the concept of sparse Volterra series [11] and of a multi-input Volterra series formulation including the so-called cross kernels [9].

Reduced-order models using neural networks have also succeeded in predicting nonlinear unsteady aerodynamic loads and, distinctly, in modeling aeroelastic limit-cycle oscillations. Several neural network architectures have been applied to these intents, e.g., radial basis function neural networks (RBFNN) [10, 14, 15], discrete-time recurrent neural networks (DTRNN) [16], local linear neuro-fuzzy models [17], and finite impulse response (FIR) neural networks [18]. Specifically, casting temporal neural networks as multilayer functionals [18] holds its relation to Volterra series, as both being functional form representations of nonlinear systems.

The models produced by neural networks, however, can be to some extent opaque. The reason regards the fact that neural networks do not show a direct correlation between their

parameters and the dynamic characteristics of the nonlinear system under analysis. Thereof arises one of the particular advantages in representing a system through a Volterra series, as their kernels have physical meaning. Besides, Volterra series can be readily transformed to bilinear state space form [19] and are well defined in the frequency domain. In Ref. [20], the relation between nonlinear autoregressive exogenous (NARX) neural networks and Volterra series is explored for obtention of higher-order frequency response functions, the kernels analogs in frequency-domain.

The purpose of this work is to apply a kernel extraction technique based on time-delay neural networks (TDNNs) to the modeling of nonlinear aerodynamic loads. The validity of this methodology will be evaluated through comparison with classical impulse-type kernels identification technique, since no analytical kernels can be derived for the aerodynamic regime considered. Details on the theory of Volterra kernel assessment from the internal parameters of time-delay neural networks are presented and their application to nonlinear aerodynamic systems is demonstrated for prescribed harmonic motions in both pitch and plunge degrees of freedom for the NACA0012 airfoil.

III. Volterra Series Mathematical Model

Any time-invariant, fading memory, nonlinear system can have the relation between its output $y[n]$ and its input $u[n]$ expressed by a Volterra series [21]. The discrete-time formulation for a single-input finite memory system is given by

$$y[n] = h_0 + \sum_{k=n-n_1}^{n} h_1[k]u[n-k] + \sum_{k_1=n-n_2}^{n}\sum_{k_2=n-n_2}^{n} h_2[k_1,k_2]u[n-k_1]u[n-k_2] + \ldots + \\ + \sum_{k_1=n-n_p}^{n} \cdots \sum_{k_n=n-n_p}^{n} h_p[k_1,k_2,\ldots,k_p]u[n-k_1]u[n-k_2]\ldots u[n-k_p] + \\ \ldots \tag{1}$$

where $n = 0,1,2,\ldots$ is the discrete-time index, $h_p[k_1, k_2, \ldots, k_p]$ is the p^{th}-order Volterra kernel, and n_p is the length of the p^{th}-order kernel. The kernel length is a measure of the time required for the effect in the system response of a past input to disappear, i.e., a measure of the required memory length, and must be estimated for each kernel function [22]. The system steady-state response h_0 is assumed zero with no loss of generality.

The identification of the kernel functions is central to obtaining an accurate Volterra series representation. Once these functions are known, it is possible to predict the nonlinear system response to any arbitrary input. Classical kernel identification is based on applying impulse inputs of various orders. By assuming that the system is weakly nonlinear [23], a suitable representation can be obtained retaining only the first two kernels of the series. The discrete-

time kernels of a truncated, second-order Volterra series identified with an impulse function of magnitude ξ_0, are given by

$$h_1[k] = \frac{1}{\xi_0}\left(2y_0[k] - \frac{1}{2}y_2[k]\right), \quad (2)$$

$$h_2[k,k] = \frac{1}{\xi_0^2}\left(\frac{1}{2}y_2[k] - y_0[k]\right), \quad (3)$$

$$h_2[k_1,k_2] = \frac{1}{2\xi_0^2}(y_1[k_1] - y_0[k_1] - y_0[k_2]), \quad (4)$$

where y_0, y_1 and y_2 are, respectively, the system's output to an impulse occurring at time k, to a double impulse occurring at times k_1 and k_2, and to an impulse of double magnitude at time k. Because the system is time-invariant, the response to a single impulse y_0 is only identified once and shifted in time. Computation of the second-order kernel is simplified given the assumed symmetry. For further details on this technique, refer to Refs. [6, 8, 23].

Equations (2) to (4) also apply if step responses are used for the identification process instead of impulse responses. The only difference lies in the convolution procedure, where the derivative of the input signal should rather be used [8].

An alternative approach to compute the kernels of a Volterra series is based on their relations with time-delay neural networks. Through this method, a generic expression can be derived to represent the p^{th}-order kernel [3]. A trained feedforward neural network composed of M + 1 input units, a single hidden layer of N hidden nodes and one output node is considered for derivation of the kernel functions. Each input unit is associated with a time delay of the input signal sampled in time, and the output node yields the current state of the system. The connection between the i^{th} input node and the j^{th} hidden unit is weighted by w_{ij}. The same applies to the links between the hidden units and the output node through the amounts c_j. The network architecture can be better understood considering Fig. 1.

The neural network admits the weighted sum of the time-delayed inputs into a hidden unit as

$$x_j = \sum_{i=0}^{M} w_{ij}u[n-i]\,. \quad (5)$$

After being biased by b_j, the sum in Eq. (5) is processed at the hidden unit with a nonlinear transfer function, which can be expanded by Taylor series. Assuming a hyperbolic tangent

transfer function and taking its Taylor expansion around the bias, the resulting polynomial for a hidden unit is

$$p_j(x_j + b_j) = tanh(x_j + b_j) = \sum_{p=0}^{\infty} \frac{tanh^{(p)}(b_j)}{p!}(x_j)^p = \sum_{p=0}^{\infty} a_{pj}(x_j)^p, \quad (6)$$

where $tanh^{(p)}$ is the p^{th} derivative of $tanh$ and a_{pj} represents the coefficients of the polynomial expansion. Calculation of the a_{pj} values can be performed analytically or using any symbolic manipulation package.

As it normally applies to function fitting problems, the output neurons have linear transfer functions. Assuming the bias $b_{out} = 0$, the output $y[n]$ of the network (*cf.* in Fig. 1) can be expressed in terms of a linear combination of the output of each hidden node, namely,

$$y[n] = \sum_{j=1}^{N} c_j p_j(x_j) = \sum_{j=1}^{N} \sum_{p=0}^{\infty} c_j a_{pj}(x_j)^p . \quad (7)$$

Combining and rearranging Eqs. (5) and (7) gives

$$\begin{aligned} y[n] &= \sum_{p=0}^{\infty} \sum_{j=1}^{N} c_j a_{pj} \left(\sum_{i=0}^{M} w_{ij} u[n-i] \right)^p \\ &= \sum_{j=1}^{N} c_j a_{0j} + \sum_{j=1}^{N} c_j a_{1j} \left(\sum_{i=0}^{M} w_{ij} u[n-i] \right) + \sum_{j=1}^{N} c_j a_{2j} \left(\sum_{i=0}^{M} w_{ij} u[n-i] \right)^2 + \dots \\ &= \sum_{j=1}^{N} c_j a_{0j} + \sum_{i=0}^{M} \left(\sum_{j=1}^{N} c_j a_{1j} w_{ij} \right) u[n-i] + \sum_{i_1=0}^{M} \sum_{i_2=0}^{M} \left(\sum_{j=1}^{N} c_j a_{2j} w_{i_1 j} w_{i_2 j} \right) u[n-i_1] u[n-i_2] \\ &+ \dots \end{aligned} \quad (8)$$

This structure closely resembles the discrete-time Volterra series of Eq. (1). In fact, the Volterra kernels can be expressed in terms of the internal parameters of the neural network, according to

$$h_0 = \sum_{j=1}^{N} c_j a_{0j}, \quad (9)$$

$$h_1[i] = \sum_{j=1}^{N} c_j a_{1j} w_{ij}, \quad (10)$$

$$h_2[i_1, i_2] = \sum_{j=1}^{N} c_j a_{2j} w_{i_1 j} w_{i_2 j}, \quad (11)$$

or generally, as

$$h_p[i_1, i_2, \ldots, i_p] = \sum_{j=1}^{N} c_j a_{pj} w_{i_1 j} w_{i_2 j} \ldots w_{i_p j}, \quad (12)$$

where the number of kernel elements that can be calculated is limited by the number of input units. Such a restriction might not impose a problem for aerodynamic systems, as they typically present kernels with a quick decay [9].

Equation (12) provides a systemic framework for the extraction of the full kernels of any order. Computational demands regarding the multidimensional convolutions of high orders, i.e. over fourth or fifth order, will, however, still exist. Such demands might limit the maximum order in which the series are truncated. Moderate aerodynamic nonlinearities can be well represented within these limits. Moreover, even though the methodology provides the possibility of representing stronger nonlinearities, some classes of problems will still not possess a Volterra series representation. Systems with multiple equilibria, subharmonic generation or with chaotic motion do not obey the hypothesis of fading memory [24]. A global unique Volterra series will not exist in such cases, but a representation may be found around each different state of the system. Airfoils oscillating at high angles of attack or experiencing dynamic stall might present such kind of behavior.

IV. Reduced-Order Model of Airfoil Nonlinear Unsteady Loads

The described kernel extraction methods are studied with the NACA0012 airfoil section at compressible flow conditions. The ROMs are tested with forced harmonic oscillations around a mean angle of attack α_m at different Mach numbers (M_∞). The pitching $\Delta\alpha(\tau)$ and heaving $\Delta w(\tau)$ motions are prescribed in nondimensional time $\tau = {}^{tU_\infty}/_{c}$, where t is the time instant, U_∞ is the freestream velocity, and c is the airfoil chord length. The cases range over different displacements amplitudes and reduced frequencies, given by $k = \left({}^{\omega b}/_{U_\infty}\right)$, where ω is the angular frequency, and b is the airfoil semi-chord *{text removed}*. A subscript is used in the reduced frequency symbol to denote the degree of freedom of the motion. In heaving motion, the displacement is given in terms of the airfoil chord c. Motion is applied separately in each degree of freedom. A multi-input Volterra series formulation would be

required to correctly account for simultaneous excitation in both degrees of freedom. The test cases are summarized in Table 1, divided into two sets. The first set is composed of weakly nonlinear variations of the AGARD experimental CT2 and CT5 test cases [25]. These adaptations, as they were proposed in Ref. [9], are intended to constrain the strength of the aerodynamic nonlinearities to a level that can be well-handled by a second-order Volterra series and to introduce a forced motion in the plunge degree of freedom. They offer, therefore, a means of consistently evaluating the neural network Volterra ROM in a range that the impulse-type Volterra ROM is well-representative. The second set is complementary and introduces test cases with stronger nonlinearities, including the conditions of the AGARD CT2 and CT5 experiments themselves. These cases make possible to evaluate if the higher-order kernels obtained from the neural network are realistic and can be used in the representation of more demanding nonlinear conditions. For all the described movements, the moment coefficient C_m is measured around the quarter-chord, except for the CT2 test case for which this position is $0.273c$.

A. CFD Validation

All aerodynamic simulations were performed using an inviscid Euler CFD code [26]. The code is based on a two-dimensional solver using a finite volume discretization with an explicit second-order accurate time marching scheme. The unsteady solutions are all carried out with a nondimensional time step of $\Delta\tau = 6\times10^{-4}$. The computational domain around the NACA 0012 airfoil is composed of an unstructured triangular O-type mesh with 19,886 elements, extending 20 chords away from the profile in all directions. The first grid node off the airfoil surface in the perpendicular direction distances about $0.007c$. Adequacy of computational grid, domain extension, and time step was established following several solution independence studies presented in Ref. [26].

The validation of the CFD results was performed using the available experimental data for the CT2 and CT5 AGARD test cases [25], whose parameters can be found in Table 1. Figure 2 shows that a reasonable match was obtained between the numerical simulations and the wind-tunnel data for both normal force and pitching moment coefficients, C_n and C_m, at two Mach numbers, namely, 0.6 and 0.755. The errors observed may be due to the Euler's formulation characteristic neglect of the viscous effects and to uncertainties in the experimental measurements. The results are also similar to simulations performed using other CFD approaches [27].

B. Impulsive Kernel Identification

The kernel identification using impulse responses of various orders employs Eqs. (2) to (4). An impulse amplitude of $\xi_0 = 0.25°$ is used for the identification in the pitch degree of freedom. In heave, more precise ROMs could be obtained by applying impulses relatively to the velocity response, which correspond to step inputs in the displacement. This is a more appropriate approach because the aerodynamic loading depends directly on the heave velocity, $\dot{w}$, rather than on the heave displacement, w, as recalled by the potential theory. The selected magnitude for the steps is of $\xi_0 = 0.001$ m. In all cases, the impulse response is recorded at a sample period of 1.2 in nondimensional time units, which yields about 42 points per cycle of motion. A sample period of 0.6 was employed for the periodic test cases

oscillating at higher reduced frequencies, i.e. $k = 0.2$. The impulse inputs are, therefore, applied over a duration equal to the sample period, similar to the approach used in Ref. [28]. Effectively, it implies that the impulses are ramped over a number of CFD integration time steps. This approximation of the impulse function was necessary due to the very small integration time steps, in the order of $\Delta\tau = 10^{-}3$, required to guarantee the stability of the CFD solution and, thereby avoid disturbances caused by the grid displacement that could not be accurately propagated by the numerical scheme [8]. The impulsive perturbations were applied around the flow-field mean angle of attack described in Table 1. The values of the selected impulse amplitudes and sample periods were based on error analysis. For the second-order kernel, a total of ten components were identified. Figure 3(a) illustrates the shape of the impulse inputs. The resulting aerodynamic responses of Fig. 3(b) represent the signals combined to construct the first-order kernel and the first four components of the second-order kernel in the conditions of test case 1. The moment coefficients are presented with the steady-state value subtracted. Although only a nondimensional time window of length 15 is shown, data is collected during a total interval of length 80.

C. Neural Network Training Procedure

The neural network was trained with CFD data consisting of random-phase multisine pitching or heaving motion of the form,

$$g(t) = \sum_{k=1}^{F} A_k \cos\left(2\pi f_0 k t + \phi_k\right), \quad (13)$$

where A_k is the randomly distributed motion amplitude, f_0 is the frequency band, t is the evaluated time instant, ϕ_k is the randomly distributed phase shift in the interval $[0,2\pi)$, and F is the index related to the value of the maximum frequency excited. The frequency band can be related to the number of time samples N_s that compose the signal by $f_0 = 1/(N_s\Delta t)$, where Δt is the time step used in the signal's discretization. The motion input into the CFD was scaled by a selected factor, A_n, according to $A_n \cdot g(t)/rms(g(t))$, to impose a root mean square value at a level similar to the signals of the test cases. Such an scaling ensures that the nonlinearities will be constrained within a desired level. For most cases, the A_n value assumed was about 1.5.

The training dataset was composed of time series of the angle of attack or heave velocity and the corresponding lift force or pitching moment coefficients, C_l and C_m, respectively. The size of the training sets vary from 250 to 2000 points sampled from the CFD full simulation signal at the same period over which the impulses were applied. At least one training set is generated for each degree of freedom and each condition of Mach number and mean angle of attack. A total of 4 training datasets were used. Unlike other parameters of the neural network, increasing the training set improves the accuracy of the solution. Neural networks with a total of $M = 20$ to 25 time delayed inputs and $N = 4$ to 10 hidden neurons were trained for a sufficient number of iterations using the Bayesian-regularization algorithm. The stopping criterion was based on the convergence of the mean squared error between the predicted output and the actual response, or the convergence of the number of effectively

used parameters. The Bayesian regularization takes place within the Levenberg-Marquadt algorithm. It constrains the magnitudes of the neural network parameters and forces a smoother response. Typically, the performance function used for training feedforward neural networks consists simply of the mean sum of the squared network errors in the training set. With a modified performance function that also includes the mean sum of the squared neural network weights and biases, it is possible to penalize the network complexity. The coefficients associated with the linear combination of each term of the modified performance function correspond to the regularization parameters. The Bayesian statistical framework offers a formulation to determine the optimal regularization parameters in an automated fashion [29]. Regularization was needed to avoid overfitting to small training sets and to ensure good generalization properties.

Figures 4(a) and 4(b) illustrate the training dataset in the conditions of test case 1 and compare it to the correspondent neural network output after the completion of the training for the pitching moment coefficient signals. The input motion of Fig. 4(a) corresponds to the oscillations around the mean angle of attack, with the rms value after scaling also indicated. Another multisine random signal that was not part of the training set is used to show how well the trained network can generalize. Such a test, as depicted in Figs. 4(c) and 4(d), is an important feature to ensure proper identification of the Volterra kernels. In Fig. 4(e), the frequency response shows the reduced frequency band limits of the random excitation ranging approximately up to $k = 0.77$.

V. Results and Discussion

The cases indicated in Table 1 are used to compare and analyse the performance of the kernel identification approaches for weakly nonlinear test cases and cases with stronger nonlinearities. First, an example of an identified kernel is presented. The frequency responses of the first-order kernels obtained using the impulse and neural network identification techniques are compared for test case 1 at a Mach number 0.6 in Fig. 5. It can be observed that the kernels are very similar in magnitude, but with a small phase shift that increases with frequency. It can also be noted that the two kernels differ significantly at frequencies higher than the frequency content of the multisine excitation frequency, as it could be expected. In fact, the high-frequency noise covers up the kernel content if a comparison is performed directly and without any filtering in the time domain. It is also important to note that the kernels of first-order presented in all the analyses correspond to the first-order kernel of a second-order system, that is different from the first-order kernel of a first-order system [23]. The performance of the kernels of higher-order is evaluated in the following sections using convolved responses for the approximation of unsteady aerodynamic loads. Error and computational performance of the neural network ROM is also discussed.

A. Weakly Nonlinear Test Cases

Figures 6 and 7 present the pitching moment coefficient responses due to individual inputs in the pitch and plunge degrees of freedom in the conditions of test cases 1 and 2, respectively. In both cases, the second-order Volterra ROMs, regardless the extraction

method or the degree of freedom, have performed well in representing the nonlinear CFD output. In fact, the responses of the Volterra ROMs of either first- or second-order obtained from the neural network (TDNN) are very similar to those of the models identified via impulses. Additional modeling accuracy was attained including a third-order kernel, which provided an improved response that matched the direct simulation of the neural network. These kernels of higher-order were estimated from the neural network only.

From the frequency responses of the C_m signals depicted in Fig. 8, the contributions of each kernel function to the final ROM output can be outlined. The first-order kernel is directly related to the system's linear response, showing the first-order ROM a peak at the fundamental frequency only $\left(k/k_\alpha \text{ or } k/k_{\dot{w}} = 1\right)$. Summing up the second-order kernel, the components at zero $\left(k/k_\alpha \text{ or } k/k_{\dot{w}} = 0\right)$ and twice the excitation frequency $\left(k/k_\alpha \text{ or } k/k_{\dot{w}} = 2\right)$ are captured. The third-order kernel can be then further associated with responses at the fundamental frequency $\left(k/k_\alpha \text{ or } k/k_{\dot{w}} = 1\right)$ and more notably at its triple $\left(k/k_\alpha \text{ or } k/k_{\dot{w}} = 3\right)$. This behavior can be traced back to the appearance of the sinusoidal type input p times at the p^{th}-order term of the Volterra series [30]. Important conclusions can also be drawn from the time domain analyses of Figs. 6 and 7. As it can be observed, adding the second-order component provides a constant offset to the curve, a typical asymmetrical behavior of a nonlinearity with even-order terms [31]. This could be due to an asymmetry of the mean flow field ($\alpha_m = 3.16°$) around which the airfoil is oscillating.

Figure 9 depicts test case 3 and the respective results for ROMs at Mach number 0.755, for which a mean angle of attack of 0.016° was employed. As this condition corresponds to an almost symmetric mean flow-field, a nonlinearity of odd-order dominates, and the Volterra series should, therefore, have no even-order terms of significant magnitude [32]. The kernels extracted from the neural network reproduced this expected behavior and had an approximately null second-order component. The impulsive ROMs, on the other hand, have overpredicted this contribution by introducing an asymmetry in the response that can be observed in the pitching moment in Fig. 9(a). This asymmetry effect is reinforced by the frequency response of Fig. 9(b), where a peak is visible at the second harmonic for the impulse-type ROM. The main frequency components of the CFD direct simulation and the neural network ROM appear only at the fundamental frequency ($k/k_\alpha = 1$) and at the third harmonic ($k/k_\alpha = 3$).

All responses considered in these analyses are presented with the initial gradient removed from the numerical solutions and shifted in the time axis. The suppressed transient was predicted poorly by the neural networks and inflicted with noise when the simulations were performed with null initial input delay conditions, a tendency also followed by the extracted kernels regardless of the initialization condition. Attenuation of this behavior could be achieved only by neglecting the known input delay conditions and setting them to zero for the neural network training, but at the cost of a worse convergence. Moreover, the lift-force coefficients that did not feature relevant nonlinear behavior were left out of the analyses.

B. Test Cases with Stronger Nonlinearities

The contribution of the Volterra series terms of higher-order becomes more prominent when the amplitude and reduced frequency of the forced motion is increased. This effect is adequately illustrated in Fig 10(a) by the pitching moment coefficient of test case 4, where the outcome of the kernel order in the ROM approximation can be outlined by the error in the predicted amplitude of the forced motion. A better fitting of the CFD data was obtained including the convolved responses of third- and fourth-order in the reduced-order model. This result indicates the feasibility of assessing the Volterra kernels of higher-order using the method based on time-delay neural networks. Figure 10(b) presents the frequency responses for ROMs of increasing order, ensuring the capabilities of the neural network Volterra ROM in identifying the nonlinear content of the pitching moment loading response. It can be observed that the fourth harmonic ($k/k_a = 4$) can be related to the inclusion of the fourth-order kernel in the response. It also follows that although harmonics higher than the fourth are predicted by direct simulation of the neural network, they are not part of the ROM response, as they are associated with kernels of orders higher than the largest included ones.

For the most demanding test conditions, i.e., the AGARD CT2 and CT5 test cases, the kernels of higher-order play a major role in the approximation. From the lift-force coefficient illustrated in Fig. 11(a), it can be noted that the CT2 test case presents nonlinear features more significantly at the most pronounced pitch up phase of the motion. An adequate prediction of this region was attained only with the Volterra ROM of fourth-order. For the CT5 test case, on the order hand, a linear approach is sufficient for an adequate prediction of the lift-force coefficient, as depicted in Fig. 11(b). Indeed, there was no impact in increasing the approximation order of the neural network Volterra ROM, being all the other curves coincident. Following the observations of previous test cases, the impulse-type Volterra ROM overpredicted the second-order component of the response at this symmetric mean-flow condition.

Some of the observations as mentioned earlier are also applicable for the pitching moment coefficient analyses. For both test cases, as displayed in Figs. 12 and 13, only the models of higher-order, i.e., third- and fourth-order, performed well in representing the stronger nonlinearities. The second-order truncated impulse-type Volterra ROM and the approximations of second-order in general give a poor prediction of the response, with an accentuated asymmetrical behavior at both Mach numbers. Adequate modeling, however, was attained only by training the neural network using the derivative of the angle of attack as input. The convolution procedure remained the same, except for the substitution of the α input with $\dot{\alpha}$. This change can be likely explained by the greater magnitudes of the higher-order kernels obtained when employing $\dot{\alpha}$. The small discrepancies between the convolved response of highest order and the neural network direct response are likely due to numerical inaccuracies associated with the very small magnitudes of the higher-order kernels and the time integration procedure itself.

C. Error Analyses

The modeling relative errors of the methodologies under consideration in this work are assessed for changes in the simulation parameters using,

$$\epsilon = \sqrt{\frac{\sum_{k=1}^{n} \left(y_{CFD}[k] - \tilde{y}_{ROM}[k]\right)^2}{\sum_{k=1}^{n} \left(y_{CFD}[k]\right)^2}}, \quad (14)$$

where the summation is taken only over the time period after the steady-state is achieved, y_{CFD} and $\tilde{y}_{ROM}$ are, respectively, the responses obtained directly via CFD and estimated via the Volterra ROMs.

Figure 14(a) depicts the modeling error according to the order of the Volterra ROM approximation. For the mildly nonlinear test cases (namely, cases 1 to 3 of Table 1) the errors associated with an expansion of order two or higher, for nonsymmetrical mean-flow conditions, and of order three, for symmetrical mean-flow conditions, fall within the acceptable range below 10%. By increasing the strength of the nonlinearities (*cf.* cases 4, CT2, and CT5), adequate modeling error is attained only for approximations of order three or higher. Figure 14(a) also reinforces the observed inaccuracies related to the overprediction of the magnitude of the second-harmonic by the impulse-type ROM for the symmetric mean-flow at $M_\infty = 0.755$. At these conditions, the modeling error increases for an expansion of second-order. It can be also remarked that the performance of the Volterra ROM obtained from the neural network is overall better than that of the impulse-type Volterra ROM.

Figure 14 also includes some additional error analyses of how the solution is affected by changes in the parameters of the neural network. The errors displayed in Figs. 14(b) and 14(c) refer to the neural network with the best performance out of five pieces of training for test case 1. All the training was conducted within the same data set and with random weight attribution at initialization. This was the same strategy adopted when selecting the neural network for extraction of the Volterra kernels. Regarding the number of time delays, it is shown in Fig. 14(b) that the modeling error of the neural network decays up to 15 input units and remains approximately constant above this number. A similar trend is observed for variations in the number of hidden neurons in Fig. 14(c), with a fall in the error up to five neurons. It can also be noticed an expressive error for a neural network consisting of a single neuron, as its modeling capability is limited to linear approximations. The convergence of the error despite large increases in the network size, either in the number of input units or of hidden neurons, may have been affected by the use of the Bayesian-regularization algorithm, which penalizes the network complexity when defining the weights. In general, smaller neural networks were preferred for the synthesis of the Volterra ROMs to minimize overfitting, without compromising the accuracy.

D. Computational Performance

The computational cost associated with each of the identification methodologies is of relevant importance. All simulations were performed in a cluster composed of Intel Xeon E5530 @2.4 GHz and Intel Xeon E5–2609 @1.9 GHz machines with 16 GB of RAM. The average CPU time required to compute a single impulse or step response in this machine is about 2 h 7 min. A total of 23 h 17 min of CPU time is required for the complete

identification of the model, assuming only ten components for the second-order kernel. The number of kernel components, however, might be larger if a smaller sample period is used in the identification process and the same model accuracy is desired. The total cost associated with the production of the neural-network-based Volterra ROM was mainly dominated by generation of the training signal. Adequate training performance could be achieved with CFD signals of small length that took an average of 7 h 42 min of CPU time. The time required for training the neural network and testing its convergence was of small significance. Five pieces of training of a neural network with a total of $M = 25$ time delayed inputs and $N = 10$ hidden neurons took in average less than 5 min. The values apply to ROM identification at each Mach number and mean angle of attack condition.

Once the Volterra ROMs are generated, calculation of the system response to a new arbitrary input signal using a series of second-order requires less than 1 s of CPU time. The method through which the kernel is identified has no impact on the time cost of the convolutions. The inclusion of the third- and fourth-order kernels in the responses increases the required CPU time in up to 20 s. The estimates are for computation of a nondimensional time window of length 250. For the test cases considered in Table 1, such interval yields 6 to 9 cycles of motion. For comparison, calculation of the same time window directly with CFD would require about 8 h of CPU time. Although the time cost is similar to the computational efforts of the neural-network-type ROM identification, the CFD simulation is valid for a unique input condition. The reduced-order model is much more versatile and computation of the system response in a new condition or to a new kind of input is easily performed.

VI. Conclusion

An alternative method based on the internal parameters of a time-delay neural network was tested for the identification of the Volterra series kernels. The applicability of this technique to nonlinear aerodynamic loading in the compressible flow regime was demonstrated for the NACA0012 airfoil for both pitch and plunge degrees of freedom. Responses obtained with low-order kernels (first- and second-order) were compared to their equivalents obtained from impulse-type excitations. Their expected similarity was indeed observed, with an exception at $M_\infty = 0.755$. At this Mach number, where a symmetric mean-flow condition was employed, there was an overprediction of the amplitude of the second-harmonic by the impulse-type ROM. It resulted in an unrealistic asymmetry of the response, that can be likely associated with inaccuracies of the identified second-order kernels. Such behavior was not observed for the neural network Volterra ROM. The feasibility of assessing kernels of higher-order from the parameters of the neural network was shown, as well as how they can provide additional accuracy. By employing the extracted kernels of third- and fourth-order, the possibility of adequate modeling stronger nonlinearities, such as the ones encountered in forced harmonic motions of large amplitudes or at higher Mach number conditions, was demonstrated. Regarding the frequency responses of the tested cases, a clear correlation could be established between the superharmonics predicted by the ROM and the order of the kernel functions retained in the approximation. In general, the modeling performance of the neural network Volterra ROM was equivalent or superior to the impulse-type ROM.

Acknowledgments

The authors N. de Paula and F. Marques acknowledge the financial support of the National Council for Scientific and Technological Development (CNPq) under grant numbers 131493/2016-7 and 307658/2016-3, and the São Paulo Research Foundation (FAPESP) under grant number 2017/02926-9.

I. Nomenclature

a	speed of sound
$\mathbf{a_{pj}}$	p^{th} coefficient of the polynomial expansion for the j^{th} hidden neuron
$\mathbf{A_k}$	randomly distributed motion amplitude of the multisine signal
$\mathbf{A_n}$	Amplitude scaling factor of the multisine signal
b	airfoil semi-chord
$\mathbf{b_j}$	bias of the j^{th} hidden neuron
c	airfoil chord length
$\mathbf{c_j}$	weight connecting the j^{th} hidden neuron to the output
$\mathbf{C_l}$, $\mathbf{C_m}$, $\mathbf{C_n}$	lift force, pitching moment, and normal force coefficients, respectively
$\mathbf{f_0}$	frequency band of the multisine signal, $f_0 = 1/N_s \Delta t$
F	multisine maximum excited frequency index
g	multisine motion
$\mathbf{h_p}$	p^{th}-order Volterra kernel
k	reduced frequency $k = \omega b / U_\infty$
M	number of neural network input units
$\mathbf{M_\infty}$	Mach number
n	discrete time index
$\mathbf{n_p}$	memory length of the p^{th}-order Volterra kernel
N	number of neural network hidden neurons
$\mathbf{N_s}$	number of time samples composing the multisine signal
t	continuous time
u	input of the nonlinear system

$\mathbf{U_\infty}$	freestream velocity
$\mathbf{w_{ij}}$	weight connecting the i^{th} input unit and the j^{th} hidden neuron
$\mathbf{x_j}$	weighted sum of the neural network inputs referring to the j^{th} hidden neuron
$\mathbf{y}$	output of the nonlinear system
$\mathbf{y_{CFD}}$	aerodynamic response obtained via CFD
$\tilde{y}_{ROM}$	predicted aerodynamic response using the Volterra reduced-order model
$\mathbf{\alpha_m}$	mean angle of attack
$\mathbf{\Delta\alpha, \Delta w}$	prescribed pitching and heaving motions, respectively
$\mathbf{\Delta\tau}$	nondimensional time step
$\mathbf{\epsilon}$	relative error
$\mathbf{\epsilon_0}$	magnitude of the discrete impulse
$\mathbf{\tau}$	nondimensional time, $\tau = {}^{tU_\infty}/_{c}$
$\mathbf{\phi_k}$	randomly distributed phase shift of the multisine signal
$\mathbf{\omega}$	angular frequency

References

[1]. Lucia DJ, Beran PS, and Silva WA, “Reduced-order Modeling: New Approaches for Computational Physics,” Progress in Aerospace Sciences, Vol. 40, No. 1–2, 2004, pp. 51–117. doi:10.1016/j.paerosci.2003.12.001.

[2]. Silva W, “Identification of Nonlinear Aeroelastic Systems Based on the Volterra Theory: Progress and Opportunities,” Nonlinear Dynamics, Vol. 39, No. 1–2, 2005, pp. 25–62. doi:10.1007/s11071-005-1907-z.

[3]. Wray J, and Green GGR, “Calculation of the Volterra Kernels of Non-linear Dynamic Systems Using an Artificial Neural Network,” Biological Cybernetics, Vol. 71, No. 3, 1994, pp. 187–195. doi:10.1007/BF00202758.

[4]. Soloway DI, and Bialasiewicz JT, “Neural network Modeling of Nonlinear Systems Based on Volterra Series Extension of a Linear Model,” Proceedings of the 1992 IEEE International Symposium on Intelligent Control, 1992, pp. 7–12.

[5]. Govind G, and Ramamoorthy PA, “Multi-layered Neural Networks and Volterra Series: The Missing Link,” 1990 IEEE International Conference on Systems Engineering, Pittsburgh, Pennsylvania, 1990, pp. 633–636. doi:10.1109/icsyse.1990.203237.

[6]. Rugh W, Nonlinear System Theory: the Volterra/Wiener Approach, Johns Hopkins series in information sciences and systems, Johns Hopkins University Press, Baltimore, Maryland, 1981.

[7]. Silva W, “Discrete-time Linear and Nonlinear Aerodynamic Impulse Responses for Efficient CFD Analyses,” Ph.D. thesis, College of William & Mary, Williamsburg, Virgina, 12 1997.

[8]. Raveh DE, “Reduced-Order Models for Nonlinear Unsteady Aerodynamics,” AIAA Journal, Vol. 39, No. 8, 2001, pp. 1417–1429. doi:10.2514/2.1473.

[9]. Balajewicz M, Nitzsche F, and Feszty D, “Application of Multi-Input Volterra Theory to Nonlinear Multi-Degree-of-Freedom Aerodynamic Systems,” AIAA Journal, Vol. 48, No. 1, 2010, pp. 56–62. doi:10.2514/1.38964.

[10]. Ghoreyshi M, Cummings RM, Ronch AD, and Badcock KJ, “Transonic Aerodynamic Load Modeling of X-31 Aircraft Pitching Motions,” AIAA Journal, Vol. 51, No. 10, 2013, pp. 2447–2464. doi:10.2514/1.J052309.

[11]. Balajewicz M, and Dowell E, “Reduced-Order Modeling of Flutter and Limit-Cycle Oscillations Using the Sparse Volterra Series,” Journal of Aircraft, Vol. 49, No. 6, 2012, pp. 1803–1812. doi:10.2514/1.C031637.

[12]. Prazenica RJ, and Kurdila AJ, “Multiwavelet Constructions and Volterra Kernel Identification,” Nonlinear Dynamics, Vol. 43, No. 3, 2006, pp. 277–310. doi:10.1007/s11071-006-8323-x.

[13]. Kurdila AJ, Prazenica RJ, Rediniotis O, and Strganac T, “Multiresolution Methods for Reduced-Order Models for Dynamical Systems,” Journal of Guidance, Control, and Dynamics, Vol. 24, No. 2, 2001, pp. 193–200. doi:10.2514/2.4707.

[14]. Yao W, and Liou M-S, “Reduced-order Modeling for Limit-Cycle Oscillation Using Recurrent Artificial Neural Network,” 12th AIAA Aviation Technology, Integration, and Operations (ATIO) Conference and 14th AIAA/ISSM, Indianapolis, Indiana, 2012. doi:10.2514/6.2012-5446.

[15]. Zhang W, Wang B, Ye Z, and Quan J, “Efficient Method for Limit Cycle Flutter Analysis Based on Nonlinear Aerodynamic Reduced-Order Models,” AIAA Journal, Vol. 50, No. 5, 2012, pp. 1019–1028. doi:10.2514/1.J050581.

[16]. Mannarino A, and Mantegazza P, “Nonlinear Aeroelastic Reduced Order Modeling by Recurrent Neural Networks,” Journal of Fluids and Structures, Vol. 48, 2014, pp. 103–121. doi:10.1016/j.jfluidstructs.2014.02.016.

[17]. Winter M, and Breitsamter C, “Efficient Unsteady Aerodynamic Loads Prediction Based on Nonlinear System Identification and Proper Orthogonal Decomposition,” Journal of Fluids and Structures, Vol. 67, 2016, pp. 1–21. doi:10.1016/j.jfluidstructs.2016.08.009.

[18]. Marques FD, and Anderson J, “Identification and Prediction of Unsteady Transonic Aerodynamic Loads by Multi-Layer Functionals,” Journal of Fluids and Structures, Vol. 15, 2001, pp. 83–106. doi:10.1006/jfls.2000.0321.

[19]. Kvaternik RG, and Silva WA, “A Computational Procedure for Identifying Bilinear Representations of Nonlinear Systems Using Volterra Kernels,” Tech. Rep. NASA/TM-2008–215320, NASA, Hampton,Virginia, 6 2008.

[20]. Chance J, Worden K, and Tomlinson G, “Frequency Domain Analysis of NARX Neural Networks,” Journal of Sound and Vibration, Vol. 213, No. 5, 1998, pp. 915–941. doi:10.1006/jsvi.1998.1539.

[21]. Schetzen M, The Volterra and Wiener Theories of Nonlinear Systems, Krieger Publishing, 2006.

[22]. Munteanu SL, Rajadas J, Nam C, and Chattopadhyay A, “Reduced-Order-Model Approach for Aeroelastic Analysis Involving Aerodynamic and Structural Nonlinearities,” AIAA Journal, Vol. 43, No. 3, 2005, pp. 560–571. doi:10.2514/1.10971.

[23]. Silva W, “A Methodology for Using Nonlinear Aerodynamics in Aeroservoelastic Analysis and Design,” 32nd Structures, Structural Dynamics, and Materials Conference, Baltimore, Maryland, 1991, p. 1110. doi:10.2514/6.1991-1110.

[24]. Boaghe OM, and Billings SA, “Subharmonic Oscillation Modeling and MISO Volterra Series,” IEEE Transactions on Circuits and Systems I: Fundamental Theory and Applications, Vol. 50, No. 7, 2003, pp. 877–884. doi:10.1109/TCSI.2003.813965.

[25]. “Compendium of Unsteady Aerodynamic Measurements,” Tech. Rep. R-702, AGARD, 1982.

[26]. Camilo E, Marques FD, and Azevedo JLF, “Hopf Bifurcation Analysis of Typical Sections with Structural Nonlinearities in Transonic Flow,” Aerospace Science and Technology, Vol. 30, No. 1, 2013, pp. 163–174. doi:10.1016/j.ast.2013.07.013.

[27]. Dubuc L, Cantariti E, Woodgate M, Gribben B, Badcock KJ, and Richards BE, “Solution of the Unsteady Euler Equations Using an Implicit Dual-Time Method,” AIAA Journal, Vol. 36, No. 8, 1998, pp. 1417–1424. doi:10.2514/3.13984.

[28]. Grewal A, and Zimcik D, “Application of Reduced Order Modelling to Fluid-Structure Interaction Analysis,” 12th AIAA/ISSMO Multidisciplinary Analysis and Optimization Conference, Victoria, British Columbia, Canada, 2008, p. 5961. doi:10.2514/6.2008-5961.

[29]. Hagan MT, Demuth HB, and Beale MH, Neural Network Design, 2014. doi: 10.1007/1-84628-303-5.

[30]. Balajewicz M, “On the Application of Multi-Input Volterra Theory to Nonlinear Multi-Degree-of-Freedom Aerodynamic Systems,” Master’s thesis, Carleton University, Ottawa, Canada, 8 2007.

[31]. Pearson RK, Discrete-time Dynamic Models, Oxford University Press, 1999.

[32]. Marzocca P, Librescu L, and Silva W, “Volterra Series Approach for Nonlinear Aeroelastic Response of 2-D Lifting Surfaces,” 19th AIAA Applied Aerodynamics Conference, Seattle, WA, 2001, p. 1459. doi:10.2514/6.2001-1459.

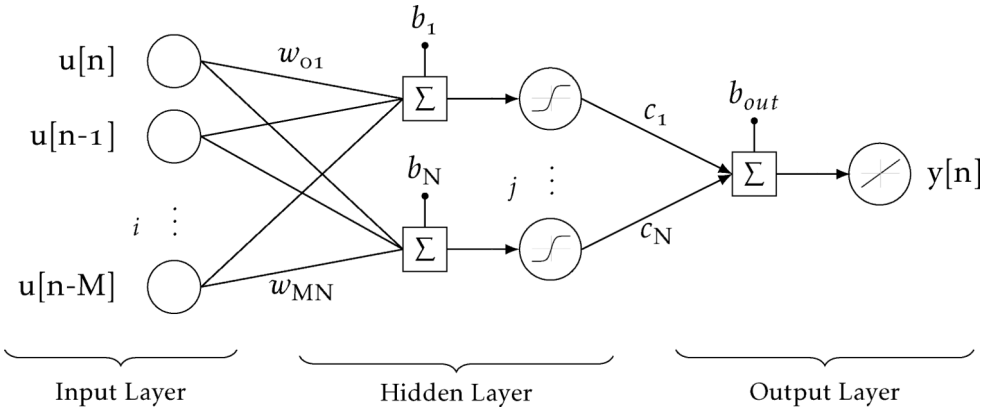

Fig. 1.
Architecture of the time-delay neural network.

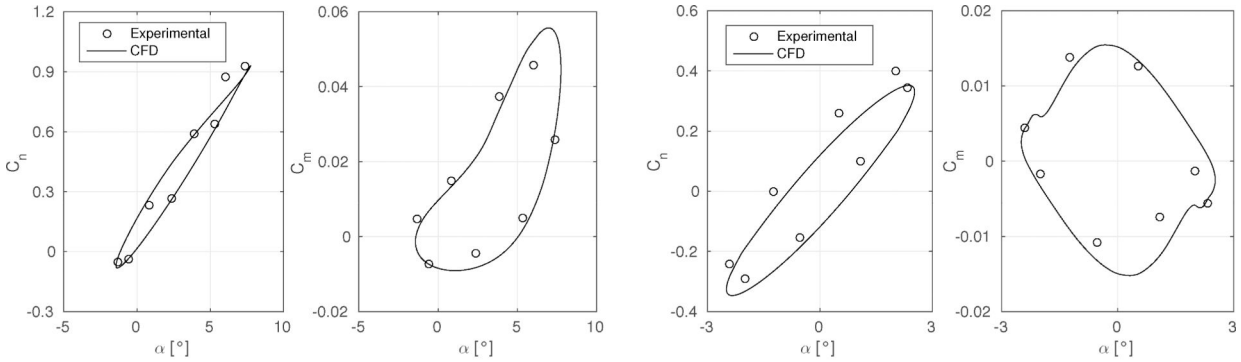

Fig. 2.
CFD validation using AGARD test cases [25].

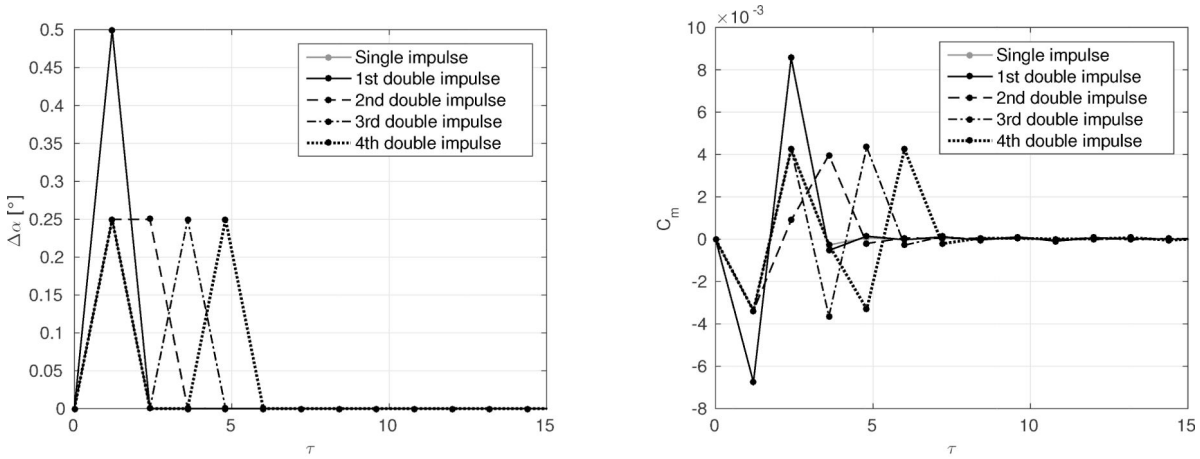

(a) Impulse inputs (b) Impulse responses

Fig. 3.

Features of the impulse inputs and responses. The signals shown correspond to the data required for the construction of the first-order kernel and the first four components of the second-order kernel. The (·) symbol denotes the data recorded with the chosen sample period.

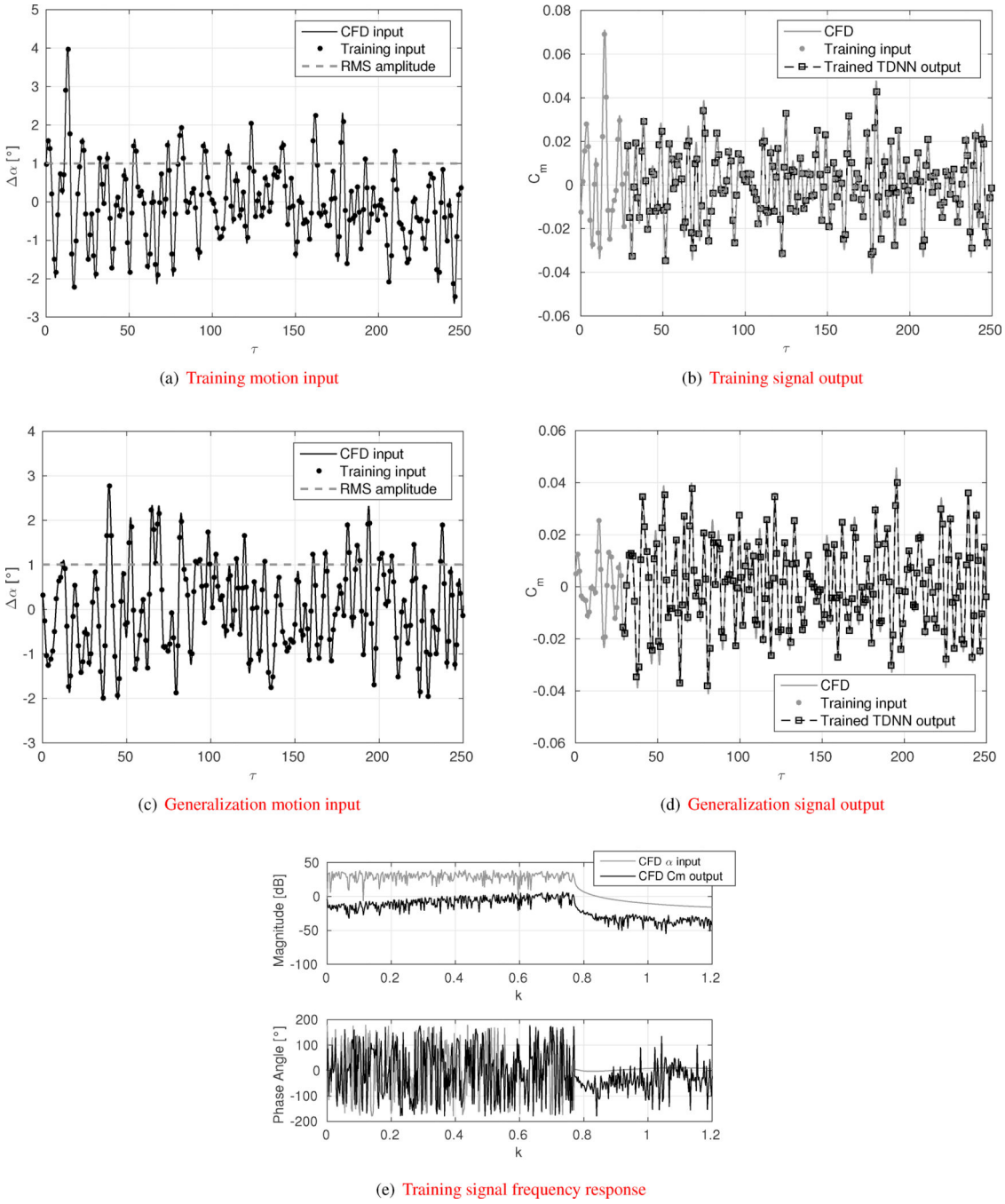

Fig. 4.

Features of the training and generalization signals obtained from the neural network (TDNN).

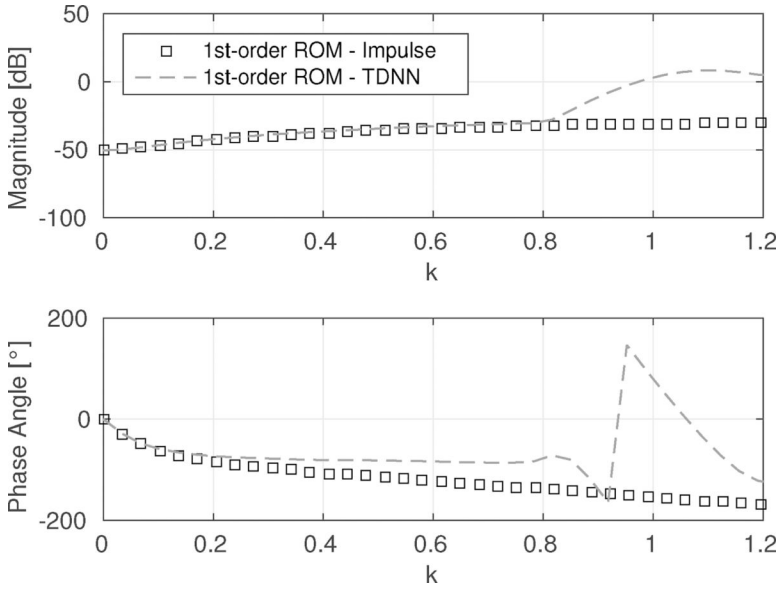

Fig. 5.

Frequency responses of the first-order kernels obtained from the impulse and the neural network techniques.

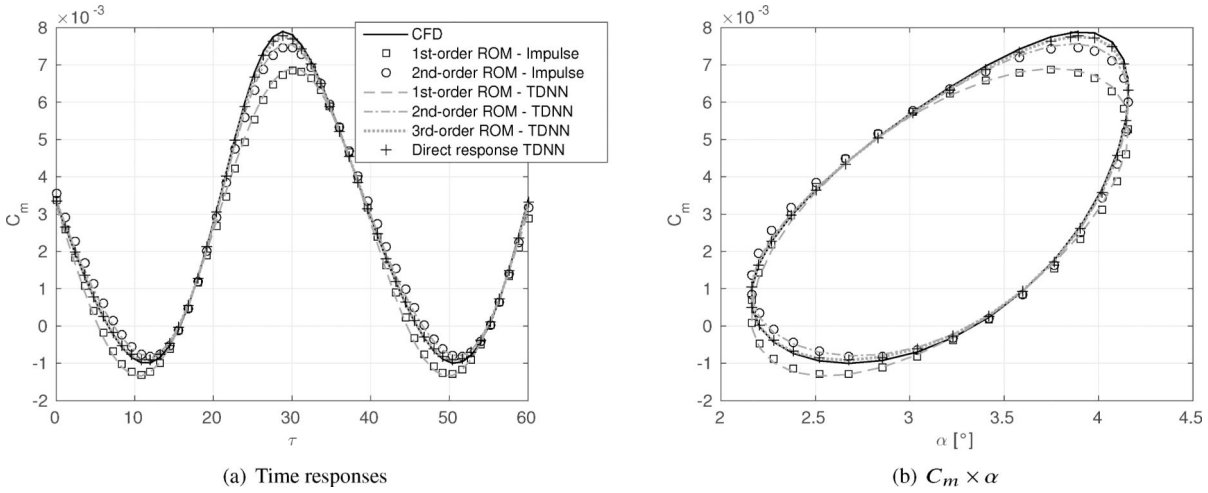

(a) Time responses (b) $C_m \times \alpha$

Fig. 6.

Pitching moment of test case 1 obtained from the Volterra ROMs due to pitch input at M_∞ = 0.6.

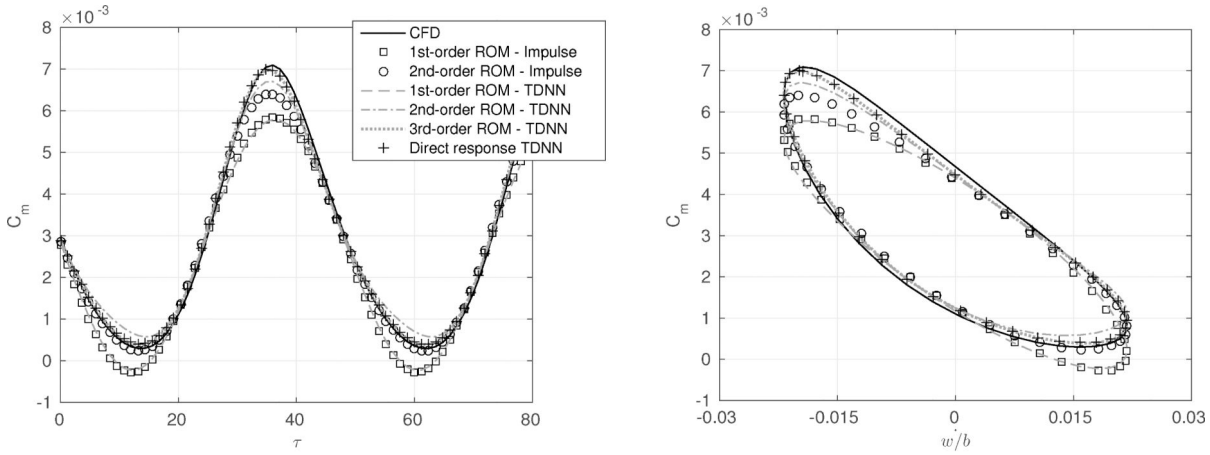

(a) Time responses (b) $C_m \times \dot{w}/b$

Fig. 7.

Pitching moment of test case 2 obtained from the Volterra ROMs due to heave input at $M_\infty = 0.6$.

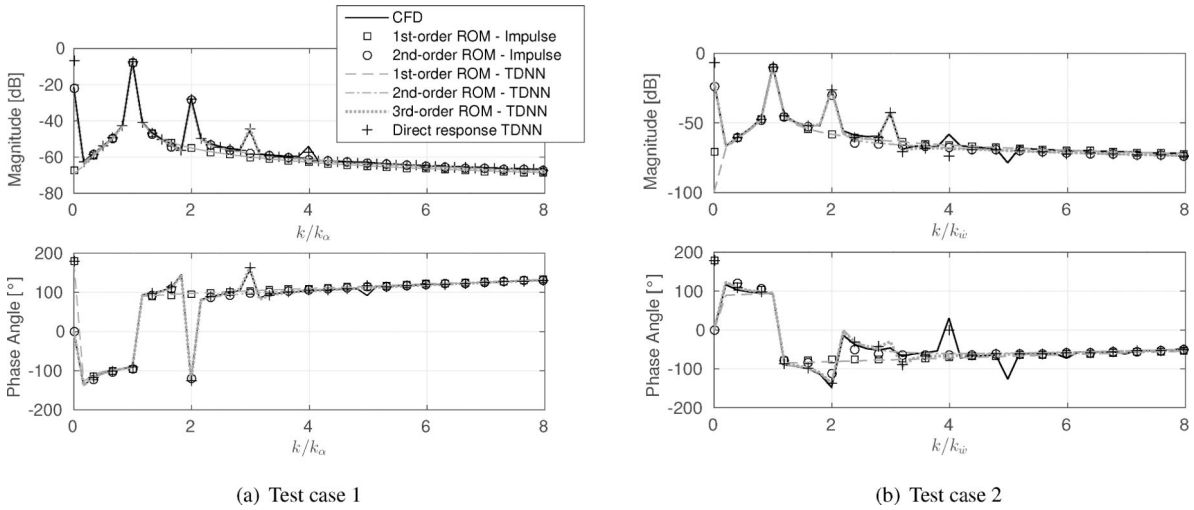

(a) Test case 1 (b) Test case 2

Fig. 8.

Frequency responses for test cases 1 and 2 obtained from the Volterra ROMs at $M_\infty = 0.6$.

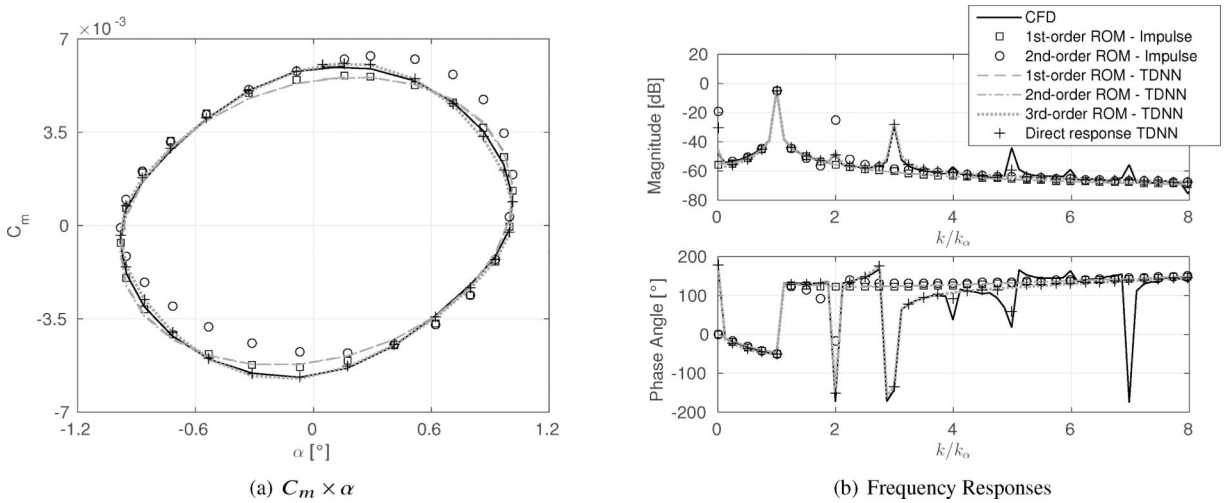

(a) $C_m \times \alpha$ (b) Frequency Responses

Fig. 9.

Pitching moment and frequency responses of test case 3 obtained from the Volterra ROMs at $M_\infty = 0.755$.

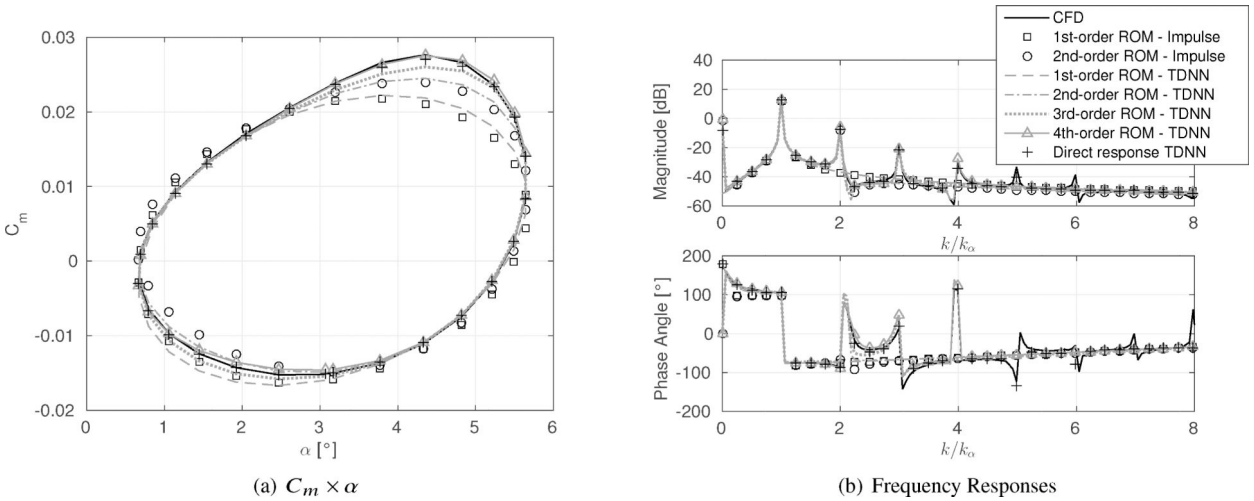

(a) $C_m \times \alpha$ (b) Frequency Responses

Fig. 10.

Pitching moment and frequency responses of the test case 4 obtained from the Volterra ROMs at $M_\infty = 0.6$.

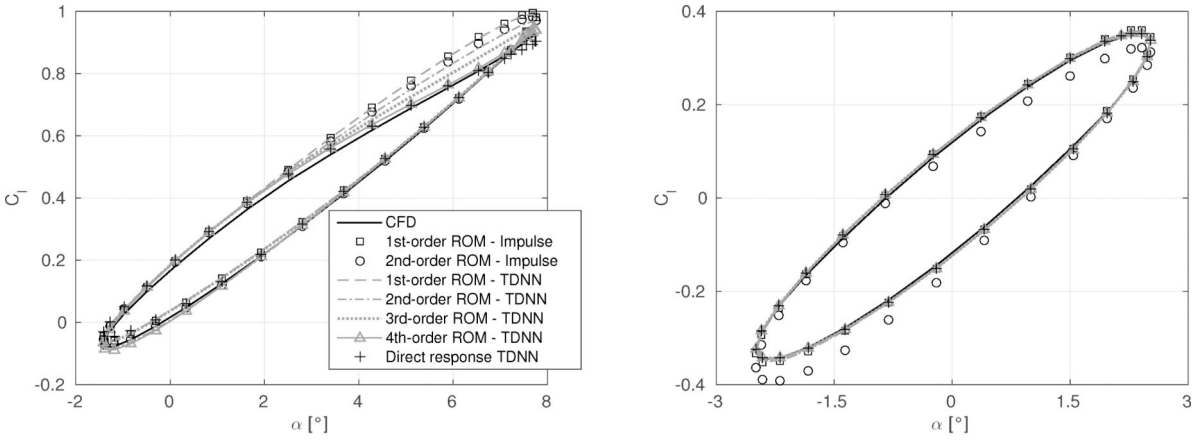

(a) CT2 (b) CT5

Fig. 11.

Lifting force for test cases CT2 ($M_\infty = 0.6$) and CT5 ($M_\infty = 0.755$) obtained from the Volterra ROMs.

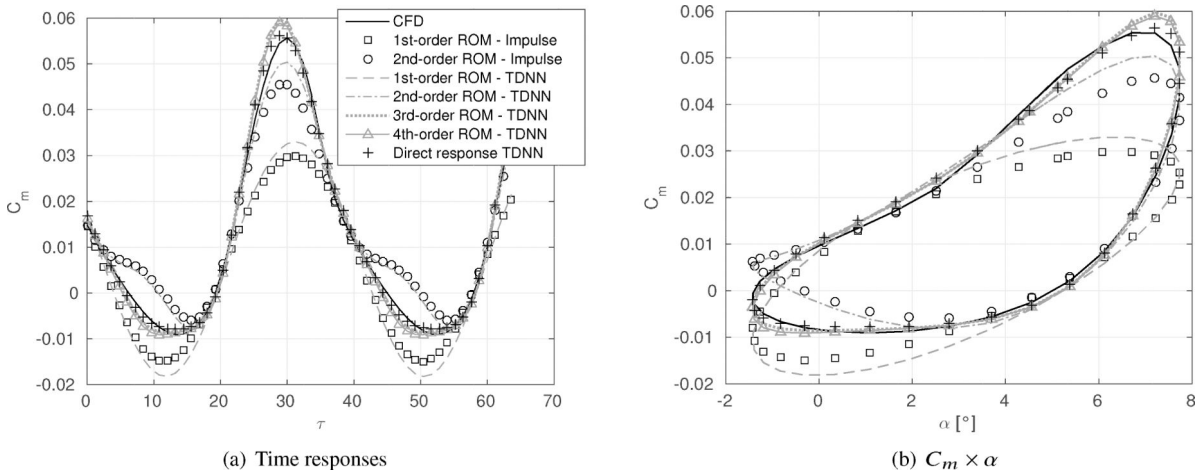

(a) Time responses (b) $C_m \times \alpha$

Fig. 12.
Pitching moment of the CT2 test case obtained from the Volterra ROMs at $M_\infty = 0.6$.

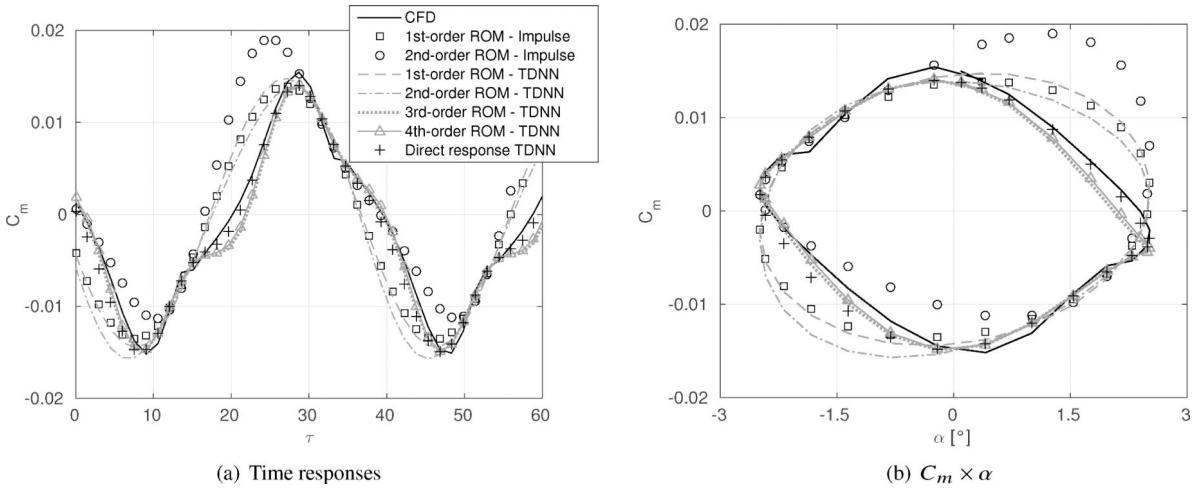

(a) Time responses (b) $C_m \times \alpha$

Fig. 13.
Pitching moment of test case CT5 obtained from the Volterra ROMs at $M_\infty = 0.755$.

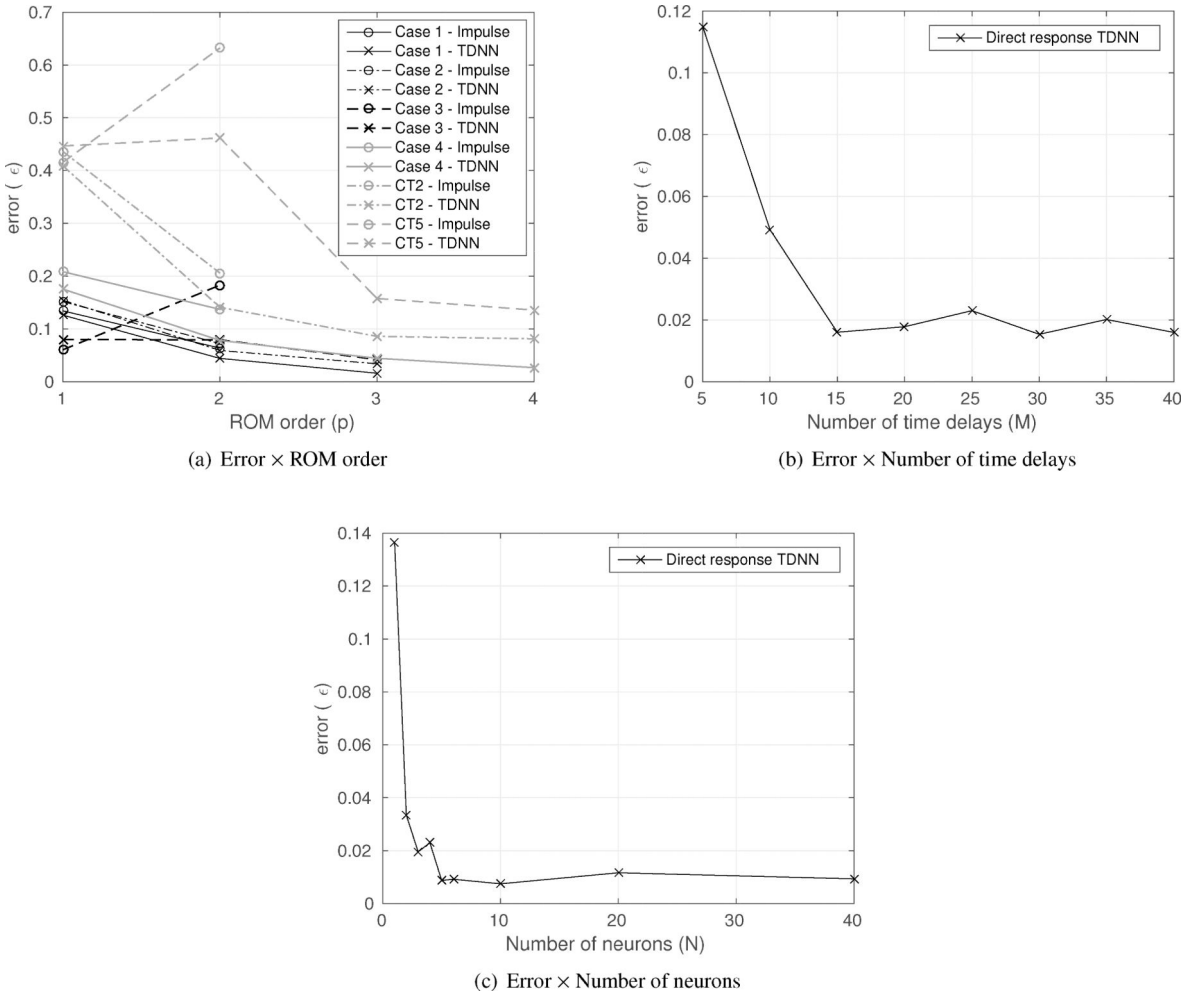

Fig. 14.

Error in C_m for variations of the neural network parameters.

Table 1

Description of the test cases.

Case	M_∞	α_m	$\Delta\alpha(\tau)$	$\Delta w(\tau)$	k
1	0.6	3.16°	$1° \sin(2k_\alpha \tau)$	[–]	0.0811
2	0.6	3.16°	[–]	$0.14c \sin(2k_w \tau)$	0.065
3	0.755	0.016°	$1° \sin(2k_\alpha \tau)$	[–]	0.0814
4	0.6	3.16°	$2.5° \sin(2k_\alpha \tau)$	[–]	0.2
CT2	0.6	3.16°	$4.59° \sin(2k_\alpha \tau)$	[–]	0.0811
CT5	0.755	0.016°	$2.51° \sin(2k_\alpha \tau)$	[–]	0.0814